New Insights into the Bacterial Targets of Antimicrobial Blue Light

Carolina dos Anjos,[a,b] Leon G. Leanse,[a,c] Martha S. Ribeiro,[d] Fábio P. Sellera,[b,e] Milena Dropa,[f] Victor E. Arana-Chavez,[g] Nilton Lincopan,[h,i] Maurício S. Baptista,[j] Fabio C. Pogliani,[b] Tianhong Dai,[a] Caetano P. Sabino[h,k]

aWellman Center for Photomedicine, Massachusetts General Hospital, Harvard Medical School, Boston, Massachusetts, USA
bDepartment of Internal Medicine, School of Veterinary Medicine and Animal Science, University of São Paulo, São Paulo, Brazil
cUniversity of Gibraltar, Europa Point Campus, Gibraltar
dCenter for Lasers and Applications, Nuclear and Energy Research Institute (IPEN-CNEN), São Paulo, Brazil
eSchool of Veterinary Medicine, Metropolitan University of Santos, Santos, Brazil
fMicroRes Laboratory, School of Public Health, University of São Paulo, São Paulo, Brazil
gDepartment of Biomaterials and Oral Biology, University of São Paulo, São Paulo, Brazil
hDepartment of Clinical and Toxicological Analysis, School of Pharmaceutical Sciences, University of São Paulo, São Paulo, Brazil
iDepartment of Microbiology, Institute for Biomedical Sciences, University of São Paulo, São Paulo, Brazil
jDepartment of Biochemistry, Institute of Chemistry, University of São Paulo, São Paulo, Brazil
kBiolambda, Scientific and Commercial Ltd., São Paulo, Brazil

Carolina dos Anjos and Leon G. Leanse contributed equally to this work. The order of the authors was determined by alphabetical order.

ABSTRACT Antimicrobial blue light (aBL) offers efficacy and safety in treating infections. However, the bacterial targets for aBL are still poorly understood and may be dependent on bacterial species. Here, we investigated the biological targets of bacterial killing by aBL (λ = 410 nm) on three pathogens: *Staphylococcus aureus*, *Escherichia coli*, and *Pseudomonas aeruginosa*. Initially, we evaluated the killing kinetics of bacteria exposed to aBL and used this information to calculate the lethal doses (LD) responsible for killing 90 and 99.9% of bacteria. We also quantified endogenous porphyrins and assessed their spatial distribution. We then quantified and suppressed reactive oxygen species (ROS) production in bacteria to investigate their role in bacterial killing by aBL. We also assessed aBL-induced DNA damage, protein carbonylation, lipid peroxidation, and membrane permeability in bacteria. Our data showed that *P. aeruginosa* was more susceptible to aBL ($LD_{99.9}$ = 54.7 J/cm²) relative to *S. aureus* ($LD_{99.9}$ = 158.9 J/cm²) and *E. coli* ($LD_{99.9}$ = 195 J/cm²). *P. aeruginosa* exhibited the highest concentration of endogenous porphyrins and level of ROS production relative to the other species. However, unlike other species, DNA degradation was not observed in *P. aeruginosa*. Sublethal doses of blue light ($<LD_{90}$) could damage the cell membrane in Gram-negative species but not in *S. aureus*. In all bacteria, oxidative damage to bacterial DNA (except *P. aeruginosa*), proteins, and lipids occurred after high aBL exposures ($>LD_{99.9}$). We conclude that the primary targets of aBL depend on the species, which are probably driven by variable antioxidant and DNA-repair mechanisms.

IMPORTANCE Antimicrobial-drug development is facing increased scrutiny following the worldwide antibiotic crisis. Scientists across the world have recognized the urgent need for new antimicrobial therapies. In this sense, antimicrobial blue light (aBL) is a promising option due to its antimicrobial properties. Although aBL can damage different cell structures, the targets responsible for bacterial inactivation have still not been completely established and require further exploration. In our study, we conducted a thorough investigation to identify the possible aBL targets and gain insights into the bactericidal effects of aBL on three relevant pathogens: *Staphylococcus aureus*, *Escherichia coli*, and *Pseudomonas aeruginosa*. This research not only adds new content to blue light studies but opens new perspectives to antimicrobial applications.

The uncontrolled spread of antimicrobial-resistant pathogens, along with delays in the discovery of novel antibiotics, has been responsible for a global public health crisis (1–3). It is estimated that antibiotic-resistant bacterial infections have been responsible for more than 1.27 million deaths worldwide in 2019 (2). As a matter of urgency, the World Health Organization (WHO) has encouraged studies focused on the discovery, research, and development of new approaches to face this unbridled threat (3).

Light-based therapies are considered promising approaches for the treatment of a myriad of diseases, including those caused by infectious agents. Although the use of light to fight infections seems to be a futuristic advance, Niels Ryberg Finsen was awarded the Nobel Prize for his contribution in using light for the treatment of infectious diseases in 1903 (4). Several recent studies have demonstrated the effectiveness of antimicrobial blue light (aBL) against a vast array of pathogens, including bacteria, algae, yeasts, and molds (5, 6). In addition, aBL has been effective against multidrug-resistant pathogens, and has also shown to be highly compatible and synergistic when applied concurrently with traditional and nontraditional antimicrobial agents (7–10). Importantly, aBL is highly selective in killing microbial pathogens over human cells, does not promote adverse effects, and the selection of resistant strains is unlikely. This makes aBL an attractive approach for clinical use (5, 6).

To date, the most accepted hypothesis is that aBL elicits its antimicrobial effects as a result of photoexcitation of endogenous chromophores (e.g., porphyrins and/or flavins) to produce cytotoxic reactive oxygen species (ROS), which trigger cellular damage to lipids and proteins (11–13). It was also suggested that a flavin photoproduct, lumichrome, may play a role as an endogenous photosensitizer that is excitable by shorter aBL wavelength (14).

Indeed, although the bacterial targets of aBL have not been fully elucidated, studies have suggested an increase in membrane permeability due to lipid peroxidation with a consequent decrease in unsaturated fatty acids (11–13). More recently, Walker and collaborators reported a two-phase protein damage/oxidative stress response to aBL in *Campylobacter jejuni*, a foodborne zoonotic pathogen (12). The authors showed that there is a specific regulation of genes that encode proteins involved in the cellular response to global protein damage, which depends on the light dose, i.e., whether it is bacteriostatic or bactericidal.

More than a century has gone by since Finsen's discovery, but the bacterial targets of aBL have yet to be fully elucidated. Therefore, in this study, we performed a robust investigation to determine the effects of aBL against bacteria of clinical interest, such as *Escherichia coli* (Gram-negative), *Pseudomonas aeruginosa* (Gram-negative), and *Staphylococcus aureus* (Gram-positive). First, we obtained the killing kinetics for bacteria exposed to aBL. We measured porphyrin content and imaged bacterial cells by fluorescence lifetime imaging microscopy (FLIM) to evaluate the spatial distribution of porphyrin content in the absence of aBL. Next, we quantified ROS formation under aBL exposure and used ROS scavengers to examine the role of singlet oxygen and hydroxyl radicals in aBL bacterial killing. To observe potential bacterial targets of aBL, we performed transmission electron microscopy (TEM). To confirm bacterial targets, we assessed DNA damage, protein carbonylation, lipid peroxidation, and membrane permeability, by comparing the three bacterial species following aBL exposure.

RESULTS

aBL effectively killed bacteria, albeit with variable efficacies. The killing curve of aBL against *P. aeruginosa*, *S. aureus, and E. coli* is exhibited in Fig. 1. For LD_{90}, we observed that *P. aeruginosa* is significantly more susceptible than *S. aureus* ($P = 0.001$) and *E. coli* ($P < 0.0001$) to aBL. Indeed, the LD_{90} and $LD_{99.9}$ for *P. aeruginosa* were 25.5 and 54.7 J/cm^2, respectively. In contrast, *S. aureus* and *E. coli* were equally tolerant to
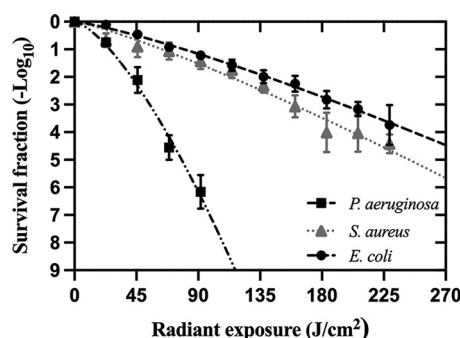
FIG 1 Dose-response curves for *E. coli*, *P. aeruginosa* and *S. aureus* exposed to aBL ($\lambda = 410 \pm 10$ nm). Values are presented as means $\pm$ SEM.

aBL exposure ($P = 0.15$). Radiant exposures of 63.5 and 158.9 J/cm² were required to achieve the LD_{90} and $LD_{99.9}$ for *S. aureus*, respectively. For *E. coli*, LD_{90} and $LD_{99.9}$ were 79.6 and 195 J/cm², respectively.

TEM revealed significant aBL-induced ultrastructural changes in all bacteria. Ultrastructural changes in *P. aeruginosa*, *S. aureus*, *and E. coli* exposed to LD_{90} and $LD_{99.9}$ of aBL are shown in Fig. 2 and Fig. S1 to 3. For *P. aeruginosa* exposed to LD_{90}, we observed a dense formation in the cytoplasm that suggests an agglutination of intracellular contents. When exposed to $LD_{99.9}$, we observed pronounced damages in the cell wall/membrane as well as cytosol leakage. Regarding *S. aureus*, there was vacuole formation following LD_{90}, indicating cytoplasmic damage. Increasing the aBL exposure to achieve the $LD_{99.9}$, conformational changes were perceived in the cell wall/membrane. For *E. coli*, evident aggregation of cellular content and detached membrane structures were observed. Besides that, the $LD_{99.9}$ promoted clear morphological changes, such as elongation and irregularities, suggesting damage to the cell wall/membrane.

Porphyrins were present in all bacteria tested. We observed that all species presented significant concentrations of porphyrins (Fig. 3), with coproporphyrin being the most abundant intracellular porphyrin regardless of the species. *P. aeruginosa* showed the highest concentrations (1,606.5 $\pm$ 564.06 pmol/mg), followed by *S. aureus* (516.0 $\pm$ 72.4 pmol/mg) and *E. coli* (71.9 $\pm$ 15.9 pmol/mg). *P. aeruginosa* also exhibited a moderate amount of protoporphyrin IX (113.8 $\pm$ 30.68 pmol/mg) while uroporphyrin was the
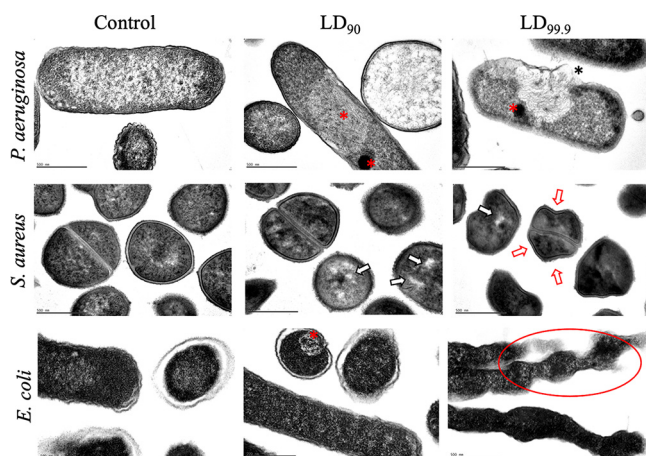
FIG 2 Representative transmission electron micrographs illustrating aBL-induced ultrastructural damages in *P. aeruginosa*, *S. aureus*, and *E. coli* for LD_{90} and $LD_{99.9}$. Red asterisk, agglutination of intracellular contents; black asterisk, cell wall/membrane damage; white arrow, leakage of intracellular contents; red arrow, membrane destabilization; red circle, elongation and morphological irregularities. Bars: 500 nm.
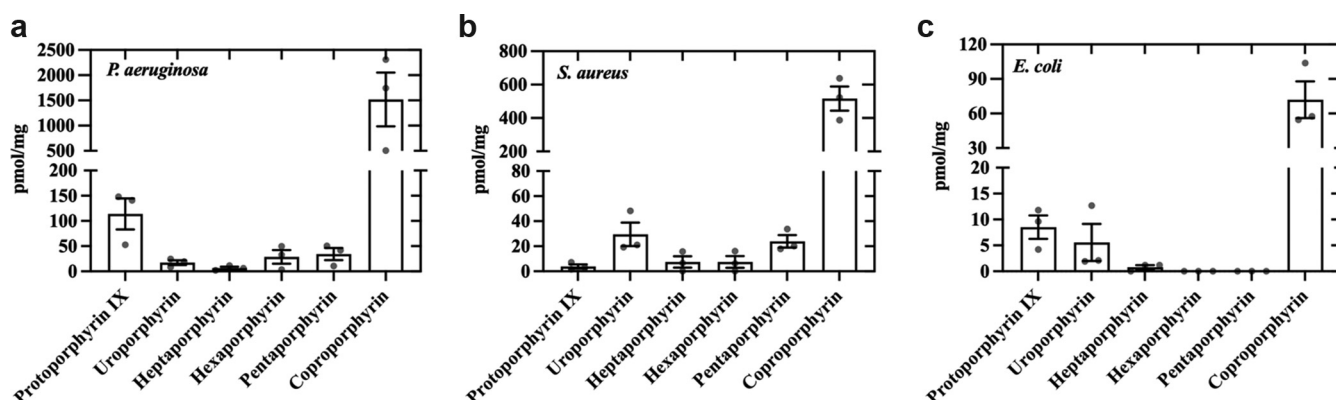
FIG 3 Porphyrin concentrations present within (a) *P. aeruginosa*, (b) *S. aureus*, and (c) *E. coli*. Symbols (●) represent the mean of three technical replicates. Data are presented as scatterplots with bar ± SEM.

second most abundant in *S. aureus* (29.5 ± 9.38 pmol/mg). Indeed, the porphyrin content of *E. coli* was much lower than that observed for *P. aeruginosa* and *S. aureus*. It is important to note that for this assay, all bacterial species were in the stationary phase of growth, because growth conditions likely affect bacteria physiology and porphyrin content may be condition-dependent.

The spatial distribution profile of intrinsic fluorophores in *S. aureus*, *E. coli*, and *P. aeruginosa* evaluated by FLIM are displayed in Fig. 4. FLIM is a unique technique that allows mapping the spatial localization of endogenous fluorophores and their interaction with biomolecules due to lifetime decay. We observed fluorophores homogeneously distrib-
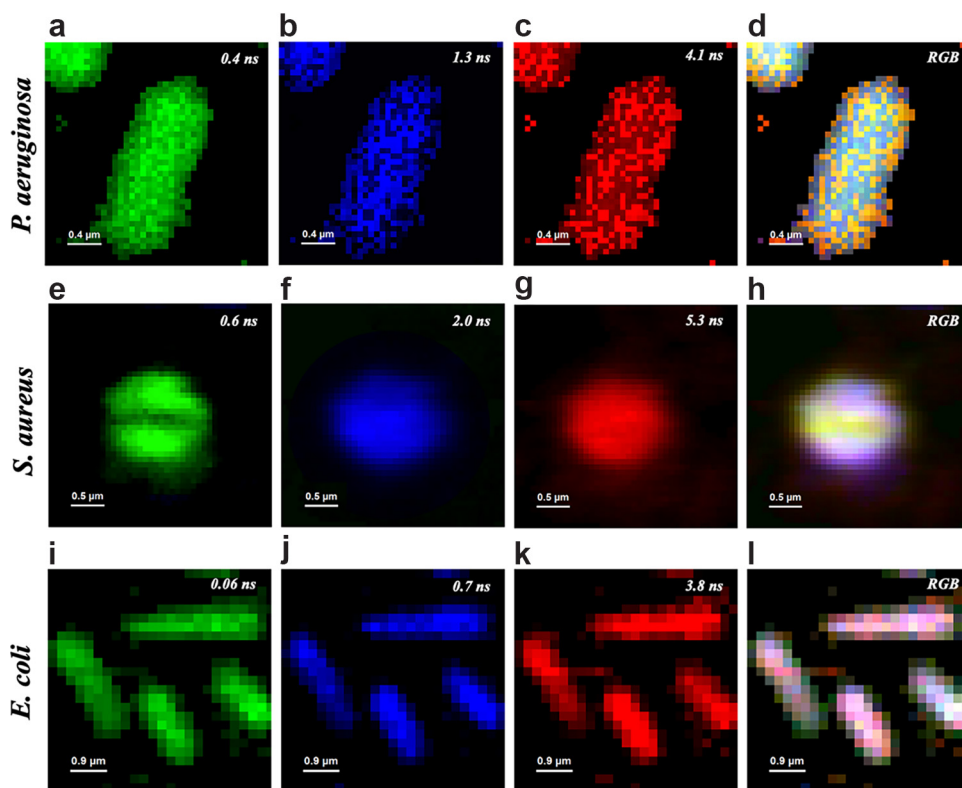
FIG 4 FLIM images of endogenous fluorophores for *P. aeruginosa* (a to d), *S. aureus* (e to h), and *E. coli* (i to l). Different colors represent different fluorescence lifetimes for each bacterial species (green < blue < red). Homogeneous distribution of fluorophores can be observed for each lifetime decay. Shorter lifetimes are observed for *E. coli*. No fluorophores were detected in the septum of *S. aureus* for the shortest lifetime (e). Merged fluorescence signal (RGB) in each bacterial species (d, h, l) is also depicted.
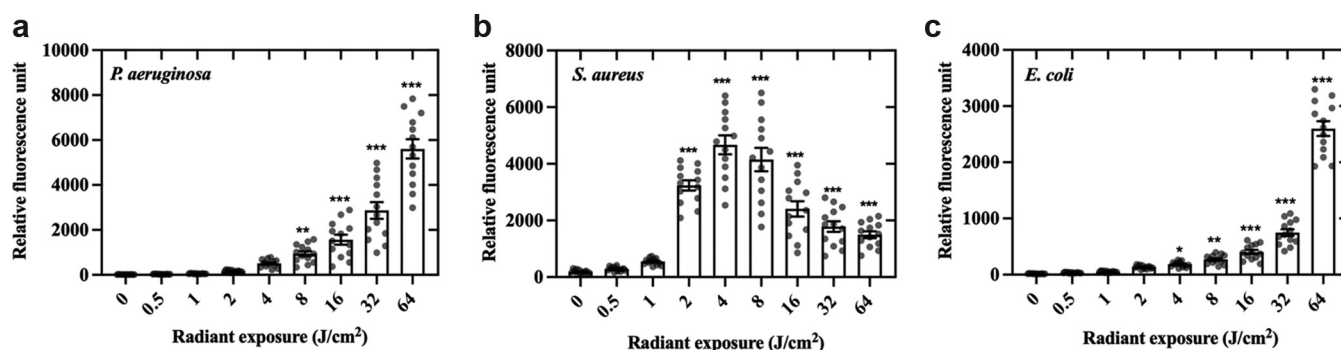
FIG 5 Relative fluorescence units proportional to intracellular ROS production in *P. aeruginosa* (a), *S. aureus* (b), and *E. coli* (c) after aBL exposure. Symbols (•) represent the average of cumulative measurements over 1 h. Data are presented as scatterplots with bar ± SEM. *, $P < 0.05$; **, $P < 0.01$; ***, $P < 0.001$ compared to unirradiated control.

uted throughout the cell due to the lack of compartmentalization of bacteria. Different fluorescence lifetimes for each bacterial species, represented by different colors, indicate either the presence of more than one fluorophore or different timespan interactions of fluorophores with intracellular components. Noteworthily, shorter fluorescence lifetimes were detected for *E. coli* regardless of the fluorophore or its interaction inside the cell. Besides, the septum dividing *S. aureus* cells appears free of fluorophores or interaction of short lifetime decay (0.6 ns) while others were detected in longer lifetimes.

aBL resulted in significant ROS production in all bacteria. We quantified ROS production as a consequence of different aBL exposures for *P. aeruginosa*, *S. aureus*, and *E. coli* by the relative fluorescence units (RFU) of oxidized DCFH-DA, which is proportional to ROS production (Fig. 5). Noteworthily, we were unable to measure ROS for *P. aeruginosa* in the absence of aBL, even though this species synthesizes pyocyanin, a redox-active compound that could react with DCFH-DA (15). Besides, *P. aeruginosa* and *E. coli* showed exponential growth of RFU dependent on the increase of the aBL radiant exposure. Indeed, the quantity of ROS was approximately 2-fold higher for *P. aeruginosa* than *E. coli* following 64 J/cm^2 (5,606 ± 308 × 2,617 ± 128, respectively). Curiously, the behavior is completely different for *S. aureus*. In this case, ROS production reaches a peak at 4 J/cm^2 (4,670 ± 486) and gradually decreases until 64 J/cm^2 (1498 ± 80).

Hydroxyl radicals and singlet oxygen played a role in aBL effect. Azide (N$_3$-) is an efficient physical quencher of $^1O_2$, which is used as a reference compound to measure the oxidation kinetics of singlet oxygen (16). On the other hand, thiourea is an effective scavenger of OH•, which directly quenches Fenton-generated hydroxyl radicals (17). The contribution of singlet oxygen and hydroxyl radicals to aBL killing of *S. aureus*, *E. coli*, and *P. aeruginosa* is displayed in Fig. 6. In the presence of NaN$_3$, aBL
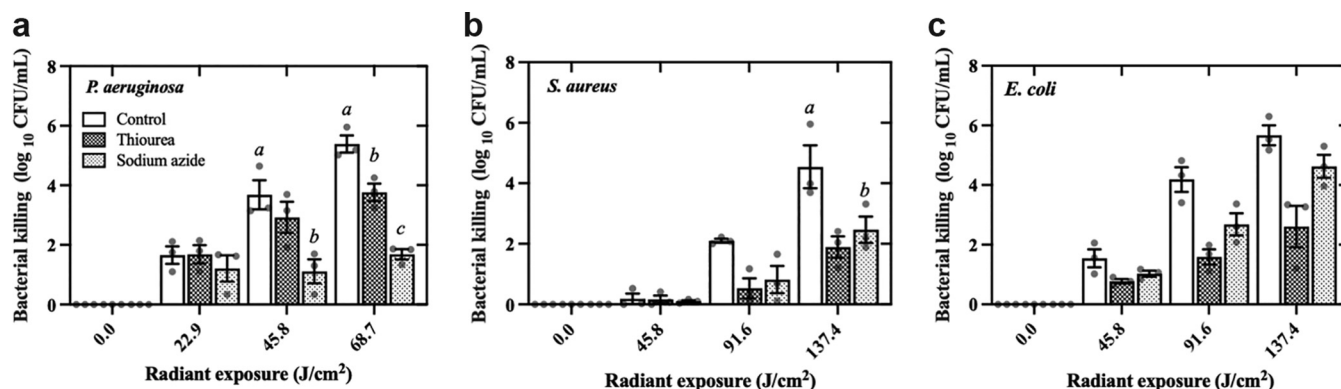
FIG 6 Effects of ROS scavengers on aBL killing of bacteria. Sodium azide (10 mM) and thiourea (150 μM) were used as scavengers of singlet oxygen and hydroxyl radicals, respectively. (a) *P. aeruginosa*, (b) *S. aureus*, and (c) *E. coli*. Symbols (•) represent the mean of three technical replicates. Data are presented as scatterplots with bar ± SEM. Different letters indicate significant differences between treatments ($P < 0.05$).
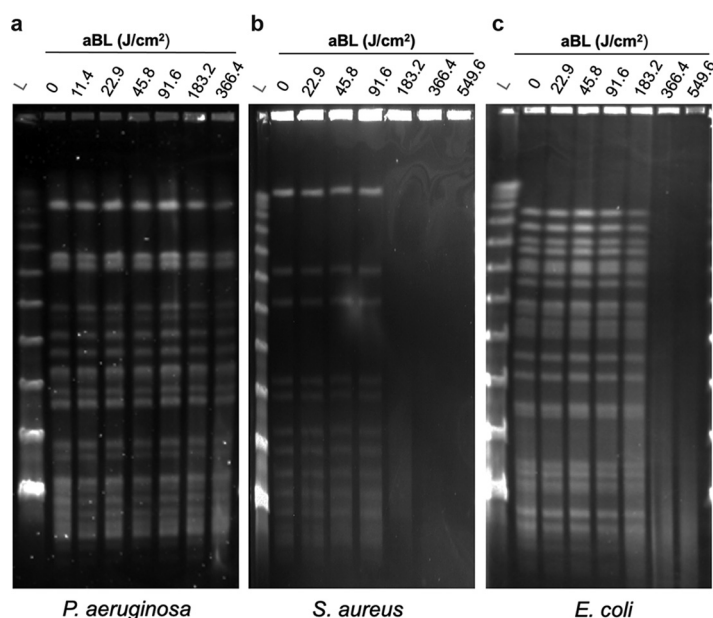
FIG 7 Analysis of DNA damage assayed by pulsed-field gel electrophoresis (PFGE) using the whole genome of *P. aeruginosa* (a), *S. aureus* (b), and *E. coli* (c). Bacterial samples were exposed to increasing radiant exposure of aBL (i.e., 0, 11.45, 22.9, 45.8, 91.6, 183.2, 366.4, and 549.6 J/cm^2), followed by DNA extraction. For DNA cleavage, specific restriction endonucleases were used for each microorganism: *XbaI*, *BcuI*, and *SmaI* for *E. coli*, *P. aeruginosa*, and *S. aureus*, respectively. The reference molecular weight ladders for pulsed-field gel electrophoresis are identified by (L).

killing of *P. aeruginosa* was significantly reduced. After 68.7 J/cm^2 of aBL exposure, lower bacterial killing (around 3-fold) was observed in the presence of NaN$_3$ (1.68 $\pm$ 0.29 log$_{10}$) than in untreated control (5.38 $\pm$ 0.49 log$_{10}$, $P = 0.002$). Although less pronounced, thiourea also promoted bacterial reduction (3.76 $\pm$ 0.50 log$_{10}$) compared to control at 68.7 J/cm^2 of aBL exposure.

For *S. aureus*, statistically significant differences in CFU reduction were only observed between NaN$_3$ and untreated control groups at aBL exposure of 137.4 J/cm^2 (2.46 $\pm$ 0.75 log$_{10}$ X 4.54 $\pm$ 1.22 log$_{10}$, $P = 0.04$). Thiourea also promoted a photoprotective effect against aBL exposure in *S. aureus* (1.88 $\pm$ 0.61 log$_{10}$) even though no statistically significant differences were detected. Regarding *E. coli*, we observed photoprotective effects of NaN$_3$ and thiourea (4.63 $\pm$ 0.57 log$_{10}$ and 2.60 $\pm$ 1.21 log$_{10}$, respectively) compared to the control (5.67 $\pm$ 0.57 log$_{10}$ of killing) but with no statistically significant differences among groups.

aBL induced DNA damages in *S. aureus* and *E. coli*, but not *P. aeruginosa*. To test our hypothesis that aBL exposure induces DNA damage in bacteria, we assessed the degradation of DNA following different radiant exposures of aBL (Fig. 7). First, we observed no DNA degradation for *P. aeruginosa*, even for the highest aBL radiant exposure (366.4 J/cm^2), able to kill 100% of bacteria (LD$_{100}$ = 117.2 J/cm^2). Second, *S. aureus* seems to be more susceptible than *E. coli* to DNA damage. Indeed, aBL exposures $\geq$183.2 J/cm^2, which is sufficient to kill over 3 log$_{10}$ CFU, (LD$_{99.9}$ = 158.99 J/cm^2), promoted significant DNA degradation in *S. aureus* whereas *E. coli* needed to be exposed to radiant exposures $\geq$366 J/cm^2 (higher than LD$_{99.9999}$ = 343.3 J/cm^2).

Bacterial proteins are susceptible to degradation by aBL at high radiant exposures. The degradation of bacterial proteins is exhibited in Fig. 8. Protein carbonylation refers to the oxidation of protein side chains to form reactive ketones or aldehydes, and its quantification allows the evaluation of the extent of oxidative stress in the context of cellular damage (18). Regardless of the species, the reduction in total protein amount or the increase in carbonylated proteins depends on the aBL radiant exposures. For *P. aeruginosa*, a significant increase in the concentration of carbonylated proteins was observed after 183.2 J/cm^2 of aBL ($P < 0.0001$). *S. aureus* and *E. coli* demonstrated reduced protein
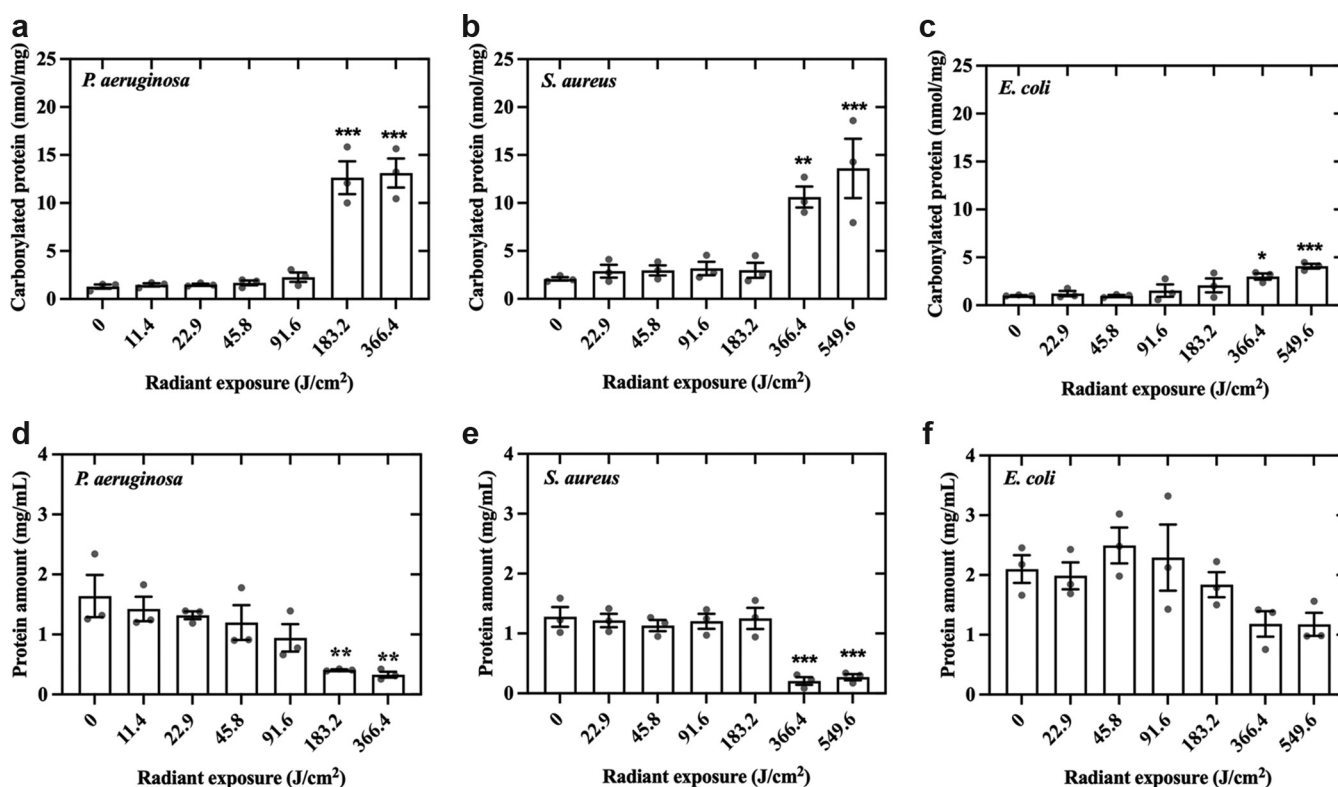
FIG 8 Effects of aBL on proteins in *P. aeruginosa*, *S. aureus*, and *E. coli* assessed by carbonyl protein quantification (a, b, and c) and total protein amount (d, e, and f). Symbols (•) represent the mean of three technical replicates. Data are presented as scatterplots with bar ± SEM. *, $P < 0.05$; **, $P < 0.01$; ***, $P < 0.001$ compared to unirradiated control.

oxidation, compared to *P. aeruginosa*, with a significant increase in carbonylated protein concentrations only after 366.4 J/cm² aBL ($P = 0.002$ and $P = 0.02$, respectively).

aBL induced lipid peroxidation in *P. aeruginosa*, *S. aureus*, and *E. coli*. Regardless of the species, the higher the dose, the greater the lipid peroxidation, which is proportional to the number of malondialdehyde groups (Fig. 9). Statistically significant differences compared to control were observed for higher aBL exposures (183.2 and 366.4 J/cm² for *P. aeruginosa*, and *S. aureus*, respectively). In contrast, lower doses of aBL (91.6 J/cm²) trigger significant lipid peroxidation in *E. coli*. Interestingly, levels of malondialdehyde (MDA) for *P. aeruginosa* are approximately 2-fold higher than for *E. coli*, regardless of the light dose.

aBL resulted in cell membrane damage in *P. aeruginosa* and *E. coli*, but not *S. aureus*. We evaluated changes to the integrity of the bacterial cell membrane using propidium iodide (PI) and N-phenyl-1-naphthylamine (NPN) (Fig. 10). For *P. aeruginosa* and *E. coli*, after 45.8 J/cm² of aBL, we observed a significant increase in NPN incorporation, indicative of membrane damage ($P < 0.01$). Similarly, a significant increase in PI incorporation was observed after the aBL exposure of 91.6 J/cm² ($P < 0.01$). In contrast, for *S. aureus*, the PI incorporation was only detected after aBL radiant exposure of 549.6 J/cm² ($P < 0.05$), which was higher than $LD_{100} = 397.7$ J/cm². On the other hand, NPN incorporation was unaltered, likely due to the structural differences in Gram-positive membranes.

DISCUSSION

Herein, we investigated the targets involved in the aBL-mediated killing of bacteria for three clinically important bacterial species: *P. aeruginosa*, *S. aureus*, and *E. coli*. Previous studies have suggested that ROS generation by aBL exposure could lead to the damage of multiple nonspecific targets, including DNA, proteins, lipids, and the cell wall/membrane (11–13).

We found differences in the efficacy of aBL among species, especially when comparing *P. aeruginosa* to *S. aureus* or *E. coli*, which are noticeably more tolerant to aBL. The
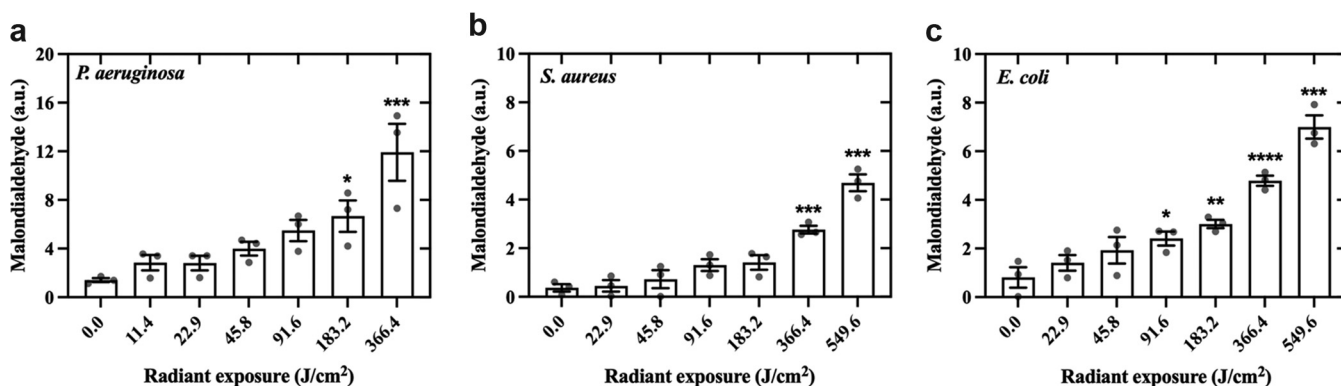
FIG 9 Effects of aBL on lipids in (a) *P. aeruginosa*, (b) *S. aureus*, and (c) *E. coli* assessed using malondialdehyde as a marker for lipid peroxidation. Symbols (●) represent the mean of three technical replicates. Data are presented as scatterplots with bar ± SEM. *, $P < 0.05$; **, $P < 0.01$; ***, $P < 0.001$ compared to the unirradiated control.

literature has pointed to porphyrins as essential intracellular chromophores that are excitable by aBL and produce ROS as a result (19–21). Therefore, a potential explanation for the different dose-response curves relies on the endogenous porphyrin concentration in each bacterial species. Thus, we quantified the endogenous porphyrins of these three species and observed that *P. aeruginosa* presents the highest concentration of porphyrins, which might explain its higher sensitivity to aBL. Interestingly, the porphyrin concentration in *S. aureus* was only 34% lower than that of *P. aeruginosa*, whereas the concentration in *E. coli* was 95% lower for *P. aeruginosa*. However, the killing observed between *S. aureus* and *E. coli* by aBL was rather similar, even though porphyrin concentration differed by 6.7-fold. This finding suggests that tolerance to aBL could not be a result of porphyrin concentration only. Indeed, Leanse et al. have reported
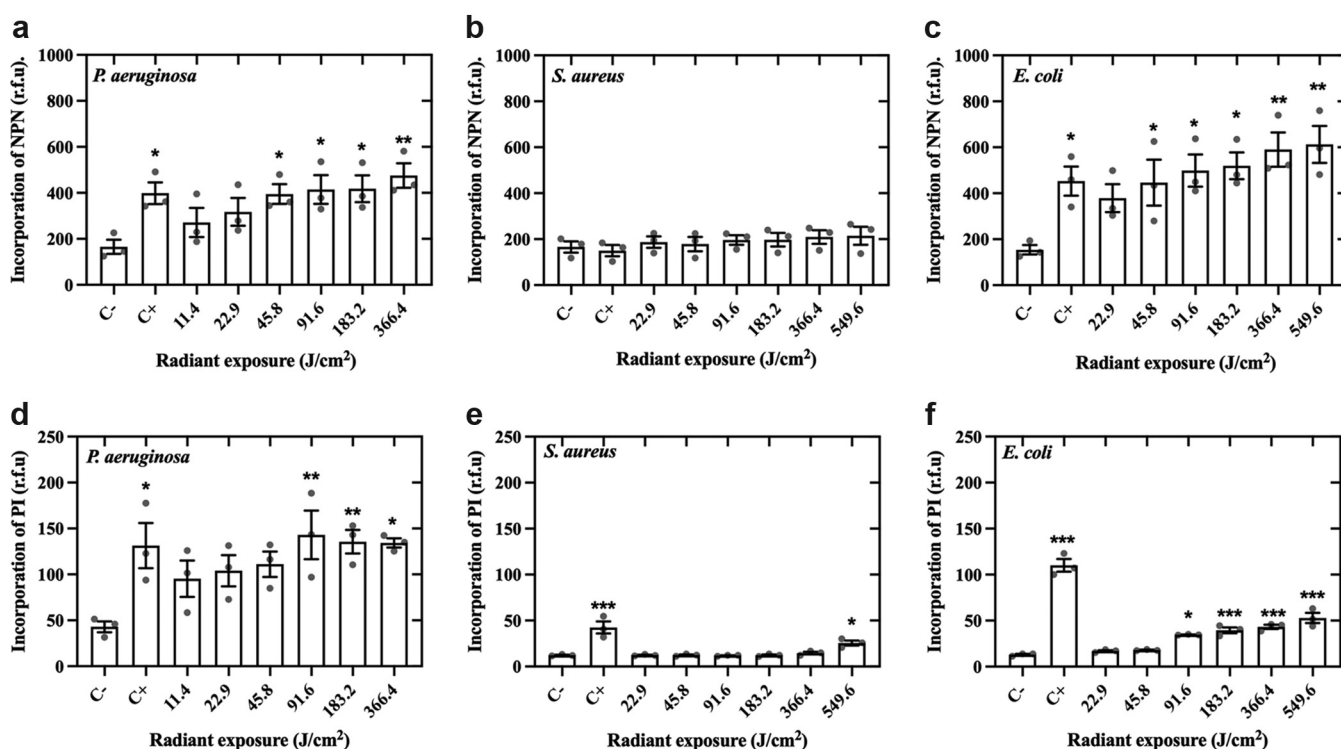
FIG 10 Effects of aBL on membrane permeabilization in *P. aeruginosa*, *S. aureus*, and *E. coli* assessed by N-phenyl-1-naphthylamine (NPN, a, b, and c) and propidium iodide (PI, d, e, and f). Symbols (●) represent the mean of three technical replicates. Data are presented as scatterplots with bar ± SEM. *, $P < 0.05$; **, $P < 0.01$; ***, $P < 0.001$ compared to the negative control (C−). Positive control (C+) for membrane damage samples were treated with ethanol at 70% for 15 min.

that the presence of the powerful antioxidant staphyloxanthin, which is a carotenoid pigment in the *S. aureus* membrane, is responsible for aBL tolerance (22). Therefore, it is likely that, while porphyrin concentration is an important factor that drives aBL efficacy, other factors such as the presence or the synthesis of antioxidant molecules may be equally essential.

We then investigated the production of ROS following increasing aBL radiant exposures for each species. For *P. aeruginosa* and *E. coli*, we observed a direct dose-response on ROS production, even though the detected ROS was remarkably lower for *E. coli*. We assume that the lower amount of endogenous porphyrins in *E. coli* is responsible for this reduced ROS production. In contrast, ROS formation by *S. aureus* reaches a peak when exposed to 4 J/cm^2. For higher radiant exposures, changes in ROS production were less pronounced. This could be explained by the antioxidant defenses of *S. aureus*, which seem to be faster triggered or more abundant than those of *P. aeruginosa* and *E. coli*. Indeed, NaN$_3$ and thiourea equally photoprotected *S. aureus* from singlet oxygen and hydroxyl radical attack. In contrast, singlet oxygen and hydroxyl radical play an important role in the killing of *P. aeruginosa* and *E. coli*, respectively.

Following exposure of bacteria to LD$_{90}$ and LD$_{99.9}$ of aBL, we observed pronounced ultrastructural damages, which were expected due to ROS production (8, 23). Cell/wall membrane showed loss of integrity in the form of rupture (*P. aeruginosa*) and conformational changes (*S. aureus* and *E. coli*). These findings are corroborated by PI staining and NPN assays. For *P. aeruginosa* and *E. coli*, sublethal doses (<LD$_{90}$) of aBL elicited significant PI and NPN incorporation, which suggests membrane permeabilization, as reported by other authors (11, 24). However, *S. aureus* showed more resistance to cell wall/membrane damage by aBL. In this case, we hypothesize that the LD$_{99.9}$ induced a conformational change in the cell wall/membrane of *S. aureus* but with no impact on the membrane permeability.

Another interesting finding is related to the quantification of lipid peroxidation by measuring MDA. Although changes in peroxidation levels have been observed, high radiant exposures were necessary to induce lipid peroxidation, which matches the results reported by Wu et al. (13). We also observed that levels of lipid peroxidation for *P. aeruginosa* are two times higher than for *E. coli* (see Fig. 9). These data could explain the membrane rupture of *P. aeruginosa* observed by TEM.

According to previous studies (25, 26), ROS production is correlated to the presence and excitation of endogenous porphyrins. Our FLIM data might therefore be associated with the localization of endogenous porphyrins. To corroborate our hypothesis, we imaged fluorescence distribution inside bacterial cells by confocal FLIM using excitation at 405 nm and emission at wavelengths longer than 590 nm. This configuration basically selects porphyrin emission because, although flavins absorb around 405 nm, their emission does not go beyond 570 nm (27). We noticed that porphyrins are uniformly distributed throughout the bacterial cell. In addition, each bacterial species presented different fluorescence lifetimes (see Fig. 4). Although these microorganisms are known to have different concentrations of intracellular porphyrins (see Fig. 3), the concentration difference cannot explain the differences in the lifetime because the fluorescence decay does not depend on the fluorophore concentration (28). As the fluorescence lifetime of intracellular porphyrins has not been fully characterized yet, the different lifetime decays observed here should indicate either the presence of different porphyrins, or different supramolecular interactions with other molecules, such as lipids, proteins and nucleic acids, suggesting different targets for aBL.

Regarding DNA, we verified that the highest radiant exposures of aBL were able to induce DNA damage in *S. aureus* and *E. coli*. Indeed, *E. coli* required about 2-fold the dose necessary to completely degrade DNA compared to *S. aureus*. To our surprise, however, there was no evidence of DNA degradation in *P. aeruginosa*, even at radiant exposures necessary to kill 100% of bacteria (around 120 J/cm^2). We suppose that the severe damage promoted by LD$_{99.9}$ in the cell membrane of *P. aeruginosa* mitigated additional damage to the DNA because ROS lifetime is quite short. DNA is an extremely

hardy molecule and sustained ROS production is likely required to elicit significant DNA degradation. On the other hand, aBL killing of *S. aureus* and *E. coli* did not result in membrane rupture, suggesting that ROS formation was sustained and contained inside the cell allowing DNA degradation.

Protein damage has also been suggested to occur as a result of aBL exposure (12). Therefore, we evaluated whether aBL could promote protein degradation. Our data showed that the total protein content of bacteria was reduced, which simultaneously increased protein carbonylation following high aBL exposures, regardless of the bacterial species. Walker et al. have suggested that protein damage through oxidation and carbonylation would be the first photodynamic effect induced by 405 nm in *C. jejuni*, given the high reaction constant of singlet oxygen with proteins (12). Other approaches to kill bacteria involving oxidative stress such as methylene-blue mediated photodynamic therapy, UV light, and ionizing radiation, can also trigger cell death by protein damage (29, 30).

It is well known that some ROS, such as singlet oxygen and hydroxyl radicals, are capable of oxidizing nearly all biological targets. However, the reaction triggers have minimal diffusion from their production site. Conversely, radicals less reactive diffuse over greater distances in the bacterial cell, being limited by physical barriers and charge interactions (31). Thus, damage in bacterial targets is based upon several factors, including the rate constant for the oxidant's reaction with the target, the location of the target relative to that of the oxidant, the occurrence of secondary damaging events, such as chain reactions or the occurrence of intra- and intermolecular reactions (29, 31). Repair mechanisms and the presence of antioxidants in the bacterial cell also influence the bacterial response (32).

It is important to highlight that, although we have compared species using ATCC strains as a standard of the field, sensitivity to aBL can also be strain-specific. Indeed, different strains of the same bacterial species show variable susceptibility to aBL depending on the strain's characteristics, such as phenotypic profile and endogenous pigments (9, 33). Thus, additional studies carried out on clinical isolates, as well as on polymicrobial communities, are welcome to improve the understanding of aBL targets.

In conclusion, our results clearly show that aBL induces significant antimicrobial effects on different bacterial species. However, we observed variable efficacy of aBL, which appears to be species-dependent and related to porphyrin concentration, antioxidant defenses, and ROS production. Our findings also suggest that the cell membrane is the preferential target of aBL for *P. aeruginosa* and *E. coli* because low radiant exposures are necessary to promote membrane damage. Additionally, although degradation of biomolecules has been detected for *S. aureus* following high doses, membrane permeabilization was only detected at doses above LD_{100}. Taken together, these findings indicate that the primary targets of aBL strongly depend on the bacterial species.

MATERIALS AND METHODS

Bacterial strains and culture conditions. We used three bacterial species acquired from the American-type culture collection (ATCC; Manassas, VA): *S. aureus* (Gram+, 25923), *E. coli* (Gram-, 25922), and *P. aeruginosa* (Gram-, 27853). These were cultured on brain heart infusion (BHI) agar or BHI broth overnight (18 h) and incubated at 37°C in a stationary or shaking incubator. Growth conditions were the same for the three bacterial species.

Light source. Bacteria were illuminated using a blue light emitting diode (LED) array (λ = 410 ± 10 nm, LEDbox, BioLambda, Brazil) to allow homogenous (>90%) exposure of microtiter plates. The irradiance was adjusted to 38.2 mW/cm². The spectral emission was confirmed by using a UV-VIS spectrophotometer (Flame, Ocean Optics, USA).

aBL killing of bacteria. Stationary-phase bacteria were cultured in 10 mL of BHI and incubated overnight (18 h) with shaking (100 rpm). After incubation, bacteria were centrifuged at 7,378 × *g* for 10 min, washed twice, and suspended in phosphate-buffered saline (PBS; dibasic phosphate = 2.65 g/L, monobasic phosphate = 0.358 g/L, NaCl = 8.183 g/L, and milli-Q water; pH 7.4). The inoculum was standardized to approximately 1 to 2 × 10⁹ CFU (CFU)/mL by turbidity of the suspension with a spectrophotometer (λ = 625 nm; optical path = 1 cm; optical density = 0.667). Subsequently, 1 mL of the bacterial suspension was transferred to 12-well microtiter plates. All strains were subjected to the following radiant exposures: 22.9, 45.8, 68.7, 91.6, 114.5, 137.5, 160.4, 183.3, 206.2, and 229.1 J/cm². The negative-control group (nonirradiated) remained in the dark during the total exposure time. Following each light dose of aBL, bacterial viability was determined by serial dilution, plating, and CFU/mL counting as described by Jett et al. (34). Survival fraction values were determined as CFU/mL averages, normalized with each respective nonirradiated group

(N_0/N; i.e., $N_0=$ initial microbial burden; $N=$ final microbial burden) and converted into $\log_{10}$. The lethal dose (LD) for a 99.9 killing rate (i.e., 3 $\log_{10}$) was calculated according to the method described by Sabino et al. (35).

Transmission electron microscopy to determine ultrastructural changes in bacteria following aBL exposure. TEM was employed to visualize the ultrastructural changes that result from aBL exposure. Radiant exposures found to kill 90 or 99.9% (LD_{90} and $LD_{99.9}$, respectively) of each bacterial species (*E. coli*, *S. aureus*, and *P. aeruginosa*) were selected for imaging using TEM. Additionally, untreated (negative) control samples ran in parallel. After aBL exposures, bacterial cells were harvested by centrifugation, fixed in 2% glutaraldehyde, and kept overnight at 4°C. The samples were then centrifuged at 10,000 g for 10 min and washed in 0.1 M sodium cacodylate buffer (pH 7.2) twice. Pellets were postfixed in 2% osmium tetroxide in sodium cacodylate buffer for 8 h. Samples were then serially dehydrated in ethanol, and embedded in Spurr resin (Tousimis, USA). Ultrathin slices (<100 nm) were cut by diamond blades of an ultramicrotome (Leica, Germany). Samples were placed on a 200-mesh copper grid, contrasted with 4% uranyl acetate for 5 min, and 0.3% lead citrate for 15 min. The observation and capture of images were performed in a transmission electron microscope (JEOL, model 1010, Tokyo, Japan), in increments of up to 100,000×, operating at 80 kV. Images obtained by TEM were selected based on the most common cell damage observed.

Porphyrin detection and quantification by ultraperformance liquid chromatography in the absence of aBL. Overnight cultures of bacteria grown in 60 mL of BHI broth (20 mL cultures × 3 in 50 mL tubes) were pelleted by centrifugation in 7,378 × *g* for 10 min, resuspended into 1-mL extraction solution (ethanol, dimethyl sulfoxide, acetic acid, 80:20:1; vol/vol/vol) and stored at −80°C. After 24 h of incubation, cells were disrupted by an ultrasonic bath at 40 kHz (Bransonic 2510R-MT, Danbury, CT) and the porphyrin-containing supernatant was recovered for quantification by ultraperformance liquid chromatography (UPLC, Waters Acquity UPLC system) analyses as performed previously (8). In brief, chromatographic marker kits that enable the detection of uroporphyrin, heptaporphyrin, hexaporphyrin, pentaporphyrin, coproporphyrin, and protoporphyrin IX were used, and the results were compared with chromatographs produced by standard porphyrins.

FLIM to identify fluorophore distribution inside the bacterial cell in the absence of aBL. Spatial localization and fluorescence lifetime of endogenous fluorophores were observed through fluorescence-lifetime imaging confocal microscopy. Overnight cultures of bacteria were harvested by centrifugation, washed twice with sterile PBS, and adjusted in PBS to $OD_{625} = 0.667$ (approximately 1 to 2 × 10^9 CFU/mL). The time-resolved fluorescence detection was carried out by a confocal laser scanning microscope (MicroTime 200, PicoQuant), equipped with laser excitation at 405 nm, photomultiplier, 590 (36) band-pass filter, short pulse (<1 ns) and ×60 magnification to analyze samples at a super-resolution level (i.e., below the light diffraction limit). The images and data were analyzed using SymPhoTime 64 software (PicoQuant, Germany).

Detection of general reactive oxygen species during aBL exposure. Intracellular ROS production was quantified with the use of the bacterial permeant probe 2′, 7′-dichlorofluorescein diacetate (DCFH-DA; D6883, Sigma-Aldrich) as described previously (13). Under normal conditions, DCFH-DA does not emit a fluorescent signal; however, once oxidized it becomes increasingly fluorescent. In this study, DCFH-DA at a final concentration of 20 μM was applied to bacteria (10^9 CFU/mL), which were incubated at 25°C for 30 min to allow permeation of the probe. Samples were then exposed to aBL over increasing radiant exposures of 0, 0.5, 1, 2, 4, 8, 16, 32, and 64 J/cm^2, and then immediately transferred to 96-well plates. Following each aliquot of aBL, fluorescence was measured every 5 min ($\lambda_{exc} = 504$ nm and λ_{em} 529 nm) on a microplate reader (Spectramax M4, Molecular Devices, Sunnyvale, CA) for a total of 1 h.

Effects of ROS scavenging on aBL efficacy. To explore the relative contributions of specific ROS on the efficacy of aBL, we exploited the use of specific ROS scavengers: sodium azide (NaN$_3$; singlet oxygen scavenger) (37) or thiourea (hydroxyl radical scavenger) (16), which were previously shown to be produced by bacteria following aBL illumination (17). Initially, stationary-phase bacteria were resuspended in PBS at 1 to 2 × 10^9 CFU/mL, and NaN$_3$ or thiourea were added to a final concentration of 10 mM and 150 μM, respectively (16, 37). The bacterial suspension (1 mL) was subsequently transferred to a 12-well microtiter plate, and aBL radiant exposures were applied based on tolerance observed with each respective species. For *S. aureus* and *E. coli*, the following aBL exposures were applied: 0, 45.8, 91.6, and 137.4 J/cm^2, and *P. aeruginosa* was exposed to 0, 22.9, 45.8, and 68.7 J/cm^2 of aBL. For negative control, all inocula were maintained in PBS under equivalent conditions. The aBL exposure and CFU/mL quantification were performed according to the previously described.

Elucidating DNA damage following aBL exposure. Pulsed-field gel electrophoresis (PFGE) analysis was performed to assess potential DNA breakages induced by aBL. Bacterial suspensions of *S. aureus*, *E. coli*, and *P. aeruginosa* were prepared as described above and exposed to increasing aBL radiant exposures of 0, 11.45, 22.9, 45.8, 91.6, 183.2, 366.4, and 549.6 J/cm^2. Following treatment, *E. coli* and *P. aeruginosa* suspensions were pelleted by centrifugation (7,378 × *g* for 10 min) and resuspended in 200 μL of TE I buffer (Tris HCl 10 mM, EDTA 1 mM, pH 7.5). For *S. aureus*, an extra step, including 4 μL lysostaphin (L-7386; Sigma) stock solution (1 mg/mL in sodium acetate 20 mM, pH 4.5) was added. Samples (8 μL) were added into 320 μL of pulsed-field agarose solution (1%; Bio-Rad, USA) at 55 to 60°C and casted into a plug mold (36). Following solidification, *E. coli* and *P. aeruginosa* sample plugs were removed and placed into a lysis buffer (EDTA 50 mM, Tris-HCl 50 mM, SDS 1%, Sarkosyl 1%, proteinase K 0.1 mg/mL, pH 7.5). *S. aureus* sample plugs were immersed into a modified lysis buffer (EDTA100 mM, Tris-HCl 6 mM, NaCl 1 M, Brij-58 0.5%, sodium deoxycholate 0.2%, N-lauroylsarcosine 0.5%, pH 7.5). All samples were incubated at 55°C for 2 h. After lysis, plugs were washed twice in milli-Q water and four times in TE I at 15-min intervals, at 55°C.

For DNA cleavage, specific restriction endonucleases were used for each microorganism: *XbaI* (ER0682, Thermo Fisher Scientific, USA), *BcuI* (ER1251, Thermo Fisher Scientific, USA), and SmaI (ER0662, Thermo Fisher Scientific, USA) for *E. coli*, *P. aeruginosa* and *S. aureus*, respectively. Plugs were transferred into tubes containing 10 U restriction enzyme in its proper buffer and incubated at 37°C for 18 h. Following the incubation, plugs and DNA ladder (Lambda PFG Ladder, New England Biolabs) were inserted into 1% agarose gel and immersed in TBE buffer (Tris-borate 45 mM, EDTA 1 mM, pH 8.0). Electrophoresis was performed using the Chef Mapper apparatus, Bio-Rad, and configured to 6 V/cm at 14°C for 22 h, with pulse intervals between 3.51 s and 30.82 s. DNA was stained with ethidium bromide (1 μg/mL) and visualized at UV light (Epi Chemi II Darkroom, UVP Bioimaging Systems).

Assessing protein damage in bacteria by aBL through total protein and carbonyl quantification. To determine whether bacterial proteins were oxidized following exposure to aBL, we quantified total protein content as well as total carbonylated protein content. Stationary-phase bacterial suspensions were prepared to 1 to 2×10^9 CFU/mL and exposed (1 mL; 12-well plates) to increasing aBL exposures of 11.4, 22.9, 45.8, 91.6, 183.2, 366.4, and 549.6 J/cm². For each bacterial species, a total of 12 technical replicates were performed and then pooled together, to collect enough bacteria for protein extraction. The bacterial pellets were then recovered by centrifugation and resuspended in a 60 μL sample diluent from the OxiSelect Protein Carbonylation Fluorimetric Assay (STA-307; Cell Biolabs Inc., USA). Cell disruption was achieved by using a probe sonic dismembrator (Model 100, Fisher Scientific, USA) for 5 s. Five cycles of pulsing-cooling were performed. The supernatants were recovered by centrifugation at 10,000 $\times$ *g* for 5 min at 4°C. A total of 50 μL were used as input and protein carbonylation analysis was performed according to the manufacturer's instructions. In parallel, the total protein present in the samples was measured using a BCA Protein Assay (Thermo Fisher Scientific, USA) to normalize carbonyl content (nmol/mL) by protein amount (mg/mL).

Lipid peroxidation following aBL exposure. The measurement of the end products of lipid peroxidation, MDA, was performed to assess possible damages induced by aBL exposure. The stationary phase of bacterial suspensions was adjusted to a bacterial concentration of approximately 1 to 2×10^9 CFU/mL and exposed to increasing exposures of aBL at 0, 11.4, 22.9, 45.8, 91.6, 183.2, 366.4, and 549.6 J/cm². Following aBL exposure, the quantification of MDA was performed using an OxiSelect TBARS Assay (STA-330; Cell BioLabs Inc., USA), according to the manufacturer's instructions. The fluorescent reaction was measured at $\lambda_{exc} = 540$ nm and λ_{em} 590 nm.

Membrane/cell wall damage following aBL exposure. To determine if the bacterial membrane/cell wall was damaged as a result of aBL exposure, two methods were employed to quantify damage, including the use of PI and NPN (38, 39). PI is a fluorochrome that binds to DNA strands but cannot pass through a healthy cytoplasmic membrane. NPN is a nonpolar probe that fluoresces strongly in phospholipid environments like the internal face of the outer membrane (OM) of Gram-negative bacteria (39, 40). Bacterial samples (as described previously) were exposed to aBL at the exposures previously calculated to reach LD_{50}, LD_{90}, and $LD_{99.9}$ killing rates. Two comparative controls were included for each species: positive membrane damage control (70% ethanol for 15 min, which is known to lyse bacterial cells [41], and negative control, untreated sample). For the PI uptake assay, samples were distributed into 96-well plates and incubated with PI (50 μg/mL; BD Pharmingen, USA) in dark for 15 min. The PI incorporation into the membrane was measured using a plate reader spectrophotometer (SpectraMax M4; Molecular Devices, USA) at $\lambda_{ex} = 520$ nm and λ_{em} 620 nm. Using a similar method, for outer membrane assay, samples were incubated with NPN 15 μM (Sigma-Aldrich, USA). The fluorescent NPN incorporation was measured at $\lambda_{ex} = 350$ nm and λ_{em} 415 nm.

Statistical analyses. All experiments with quantitative data were carried out in three replicates and performed on three separate days. Data are presented as means and standard error of the mean (SEM). Statistical analysis was performed by using one- or two-way analysis of variance (ANOVA) with Tukey as posttest comparisons. The analysis was performed by Prism 9.0 software (GraphPad, USA). Values of $P < 0.05$ were considered statistically significant.

SUPPLEMENTAL MATERIAL

Supplemental material is available online only.

SUPPLEMENTAL FILE 1, PDF file, 5.3 MB.

ACKNOWLEDGMENTS

REFERENCES

1. Tacconelli E, Carrara E, Savoldi A, Harbarth S, Mendelson M, Monnet DL, Pulcini C, Kahlmeter G, Kluytmans J, Carmeli Y, Ouellette M, Outterson K, Patel J, Cavaleri M, Cox EM, Houchens CR, Grayson ML, Hansen P, Singh N, Theuretzbacher U, Magrini N, Aboderin AO, Al-Abri SS, Awang Jalil N, Benzonana N, Bhattacharya S, Brink AJ, Burkert FR, Cars O, Cornaglia G, Dyar OJ, Friedrich AW, Gales AC, Gandra S, Giske CG, Goff DA, Goossens H, Gottlieb T, Guzman Blanco M, Hryniewicz W, Kattula D, Jinks T, Kanj SS, Kerr L, Kieny MP, Kim YS, Kozlov RS, Labarca J, Laxminarayan R, Leder K, WHO Pathogens Priority List Working Group, et al. 2018. Discovery, research, and development of new antibiotics: the WHO priority list of

antibiotic-resistant bacteria and tuberculosis. Lancet Infect Dis 18:318–327. https://doi.org/10.1016/S1473-3099(17)30753-3.

2. Antimicrobial Resistance Collaborators. 2022. Global burden of bacterial antimicrobial resistance in 2019: a systematic analysis. Lancet 399:629–655. https://doi.org/10.1016/S0140-6736(21)02724-0.

3. World Health Organization. 2022. WHO strategic priorities on antimicrobial resistance, Available at: https://www.who.int/publications/i/item/9789240041387. Accessed January 4, 2023.

4. Hönigsmann H. 2013. History of phototherapy in dermatology. Photochem Photobiol Sci 12:16–21. https://doi.org/10.1039/c2pp25120e.

5. Leanse LG, dos Anjos C, Mushtaq S, Dai T. 2022. Antimicrobial blue light: a 'Magic Bullet' for the 21st century and beyond? Adv Drug Deliv Rev 180:114057. https://doi.org/10.1016/j.addr.2021.114057.

6. Wang Y, Wang Y, Wang Y, Murray CK, Hamblin MR, Hooper DC, Dai T. 2017. Antimicrobial blue light inactivation of pathogenic microbes: state of the art. Drug Resist Updat 33-35:1–22. https://doi.org/10.1016/j.drup.2017.10.002.

7. Li Y, Wu MX. 2021. Reversal of polymicrobial biofilm tolerance to ciprofloxacin by blue light plus carvacrol. Microorganisms 9:2074. https://doi.org/10.3390/microorganisms9102074.

8. Leanse LG, dos Anjos C, Wang Y, Murray CK, Hooper DC, Dai T. 2021. Effective treatment of cutaneous mold infections by antimicrobial blue light that is potentiated by quinine. J Infect Dis 224:1069–1076. https://doi.org/10.1093/infdis/jiab058.

9. Woźniak A, Grinholc M. 2022. Combined antimicrobial blue light and antibiotics as a tool for eradication of multidrug-resistant isolates of *Pseudomonas aeruginosa* and *Staphylococcus aureus*: *in vitro* and *in vivo* studies. Antioxidants 11:1660. https://doi.org/10.3390/antiox11091660.

10. Li Y, Wu MX. 2022. Visualization and elimination of polymicrobial biofilms by a combination of ALA-carvacrol-blue light. J Photochem Photobiol B 234:112525. https://doi.org/10.1016/j.jphotobiol.2022.112525.

11. Chu Z, Hu X, Wang X, Wu J, Dai T, Wang X. 2019. Inactivation of *Cronobacter sakazakii* by blue light illumination and the resulting oxidative damage to fatty acids. Can J Microbiol 65:922–929. https://doi.org/10.1139/cjm-2019-0054.

12. Walker P, Taylor AJ, Hitchcock A, Webb JP, Green J, Weinstein J, Kelly DJ. 2022. Exploiting violet-blue light to kill *Campylobacter jejuni* : analysis of global responses, modeling of transcription factor activities, and identification of protein targets. mSystems 7. https://doi.org/10.1128/msystems.00454-22.

13. Wu J, Chu Z, Ruan Z, Wang X, Dai T, Hu X. 2018. Changes of intracellular porphyrin, reactive oxygen species, and fatty acids profiles during inactivation of methicillin-resistant *Staphylococcus aureus* by antimicrobial blue light. Front Physiol 9:1–10. https://doi.org/10.3389/fphys.2018.01658.

14. Hessling M, Wenzel U, Meurle T, Spellerberg B, Hönes K. 2020. Photoinactivation results of *Enterococcus moraviensis* with blue and violet light suggest the involvement of an unconsidered photosensitizer. Biochem Biophys Res Commun 533:813–817. https://doi.org/10.1016/j.bbrc.2020.09.091.

15. O'Malley YQ, Reszka KJ, Britigan BE. 2004. Direct oxidation of 2′,7′-dichlorodihydrofluorescein by pyocyanin and other redox-active compounds independent of reactive oxygen species production. Free Radic Biol Med 36:90–100. https://doi.org/10.1016/j.freeradbiomed.2003.09.021.

16. Kohanski MA, Dwyer DJ, Hayete B, Lawrence CA, Collins JJ. 2007. A common mechanism of cellular death induced by bactericidal antibiotics. Cell 130:797–810. https://doi.org/10.1016/j.cell.2007.06.049.

17. Fila G, Krychowiak M, Rychlowski M, Bielawski KP, Grinholc M. 2018. Antimicrobial blue light photoinactivation of *Pseudomonas aeruginosa*: quorum sensing signaling molecules, biofilm formation and pathogenicity. J Biophotonics 11:1–12.

18. Fedorova M, Bollineni RC, Hoffmann R. 2014. Protein carbonylation as a major hallmark of oxidative damage: update of analytical strategies. Mass Spectrom Rev 33:79–97. https://doi.org/10.1002/mas.21381.

19. Amin RM, Bhayana B, Hamblin MR, Dai T. 2016. Antimicrobial blue light inactivation of *Pseudomonas aeruginosa* by photo-excitation of endogenous porphyrins: *in vitro* and *in vivo* studies. Lasers Surg Med 48:562–568. https://doi.org/10.1002/lsm.22474.

20. Hamblin MR, Viveiros J, Yang C, Ahmadi A, Ganz R a, Tolkoff MJ. 2005. *Helicobacter pylori* accumulates photoactive porphyrins and is killed by visible light. Antimicrob Agents Chemother 49:2822–2827. https://doi.org/10.1128/AAC.49.7.2822-2827.2005.

21. Plavskii VY, Mikulich AV, Tretyakova AI, Leusenka IA, Plavskaya LG, Kazyuchits OA, Dobysh II, Krasnenkova TP. 2018. Porphyrins and flavins as endogenous acceptors of optical radiation of blue spectral region determining photoinactivation of microbial cells. J Photochem Photobiol B 183:172–183. https://doi.org/10.1016/j.jphotobiol.2018.04.021.

22. Leanse LG, Goh XS, Cheng J-X, Hooper DC, Dai T. 2020. Dual-wavelength photo-killing of methicillin-resistant *Staphylococcus aureus*. JCI Insight 5: e134343. https://doi.org/10.1172/jci.insight.134343.

23. Zhang Y, Zhu Y, Gupta A, Huang Y, Murray CK, Vrahas MS, Sherwood ME, Baer DG, Hamblin MR, Dai T. 2014. Antimicrobial blue light therapy for multidrug-resistant *Acinetobacter baumannii* infection in a mouse burn model: implications for prophylaxis and treatment of combat-related wound infections. J Infect Dis 209:1963–1971. https://doi.org/10.1093/infdis/jit842.

24. Hoenes K, Bauer R, Spellerberg B, Hessling M. 2021. Microbial photoinactivation by visible light results in limited loss of membrane integrity. Antibiotics 10:341. https://doi.org/10.3390/antibiotics10030341.

25. Hyun JE, Moon SK, Lee SY. 2021. Antibacterial activity and mechanism of 460–470 nm light-emitting diodes against pathogenic bacteria and spoilage bacteria at different temperatures. Food Control 123:107721. https://doi.org/10.1016/j.foodcont.2020.107721.

26. Kim MJ, Bang WS, Yuk HG. 2017. 405 $\pm$ 5 nm light emitting diode illumination causes photodynamic inactivation of Salmonella spp. on fresh-cut papaya without deterioration. Food Microbiol 62:124–132. https://doi.org/10.1016/j.fm.2016.10.002.

27. Berezin MY, Achilefu S. 2010. Fluorescence lifetime measurements and biological imaging. Chem Rev 110:2641–2684. https://doi.org/10.1021/cr900343z.

28. Becker W. 2012. Fluorescence lifetime imaging - techniques and applications. J Microsc 247:119–136. https://doi.org/10.1111/j.1365-2818.2012.03618.x.

29. Krisko A, Radman M. 2010. Protein damage and death by radiation in *Escherichia coli* and *Deinococcus radiodurans*. Proc Natl Acad Sci U S A 107:14373–14377. https://doi.org/10.1073/pnas.1009312107.

30. Sabino CP, Ribeiro MS, Wainwright M, dos Anjos C, Sellera FP, Dropa M, Nunes NB, Brancini GTP, Braga GUL, Arana-Chavez VE, Freitas RO, Lincopan N, Baptista MS. 2022. The biochemical mechanisms of antimicrobial photodynamic therapy. Photochem Photobiol https://doi.org/10.1111/Php.13685.

31. Davies MJ. 2016. Protein oxidation and peroxidation. Biochem J 473: 805–825. https://doi.org/10.1042/BJ20151227.

32. Fasnacht M, Polacek N. 2021. Oxidative stress in bacteria and the central dogma of molecular biology. Front Mol Biosci 8:1–13.

33. dos Anjos C, Sabino CP, Sellera FP, Esposito F, Pogliani FC, Lincopan N. 2020. Hypervirulent and hypermucoviscous strains of *Klebsiella pneumoniae* challenged by antimicrobial strategies using visible light. Int J Antimicrob Agents 56:106025. https://doi.org/10.1016/j.ijantimicag.2020.106025.

34. Jett BD, Hatter KL, Huycke MM, Gilmore MS. 1997. Simplified agar plate method for quantifying viable bacteria. Biotechniques 23:648–650. https://doi.org/10.2144/97234bm22.

35. Sabino CP, Wainwright M, dos Anjos C, Sellera FP, Baptista MS, Lincopan N, Ribeiro MS. 2019. Inactivation kinetics and lethal dose analysis of antimicrobial blue light and photodynamic therapy. Photodiagnosis Photodyn Ther 28:186–191. https://doi.org/10.1016/j.pdpdt.2019.08.022.

36. Mcdougal LK, Mcdougal LK, Steward CD, Steward CD, Killgore GE, Killgore GE, Chaitram JM, Chaitram JM, Mcallister SK, Mcallister SK, Tenover FC, Tenover FC. 2003. Pulsed-field gel electrophoresis typing of oxacillin-resistant *Staphylococcus aureus* isolates from the United States: establishing a national database. J Clin Microbiol 41:5113–5120. https://doi.org/10.1128/JCM.41.11.5113-5120.2003.

37. Li MY, Cline CS, Koker EB, Carmichael HH, Chignell CF, Bilski P. 2001. Quenching of singlet molecular oxygen ($^1O_2$) by azide anion in solvent mixtures. Photochem Photobiol 74:760. https://doi.org/10.1562/0031-8655(2001)074%3C0760:QOSMOO%3E2.0.CO;2.

38. Zhu X, Dong N, Wang Z, Ma Z, Zhang L, Ma Q, Shan A. 2014. Design of imperfectly amphipathic α-helical antimicrobial peptides with enhanced cell selectivity. Acta Biomater 10:244–257. https://doi.org/10.1016/j.actbio.2013.08.043.

39. Loh B, Grant C, Hancock REW. 1984. Use of the fluorescent probe 1-N-phenylnaphthylamine to study the interactions of aminoglycoside antibiotics with the outer membrane of *Pseudomonas aeruginosa*. Antimicrob Agents Chemother 26:546–551. https://doi.org/10.1128/AAC.26.4.546.

40. Träuble H, Overath P. 1973. The structure of *Escherichia coli* membranes studied by fluorescence measurements of lipid phase transitions. Biochim Biophys Acta - Biomembr 307:491–512. https://doi.org/10.1016/0005-2736(73)90296-4.

41. Ingram LO. 1981. Mechanism of lysis of *Escherichia coli* by ethanol and other chaotropic agents. J Bacteriol 146:331–336. https://doi.org/10.1128/jb.146.1.331-336.1981.